The 2010 IEEE/RSJ International Conference on
Intelligent Robots and Systems
October 18-22, 2010, Taipei, Taiwan

Robotic Manipulation of Human Red Blood Cells with Optical Tweezers for Cell Property Characterization

Youhua Tan, Dong Sun, Wenhao Huang, Jinping Cheng, and Shuk Han Cheng

Abstract—**Cell manipulation has received considerable attentions in recent years. Most of cell manipulations are performed manually without guarantee of high precision and high throughput. This paper reports our latest research on integrating robotics technologies into optical tweezers system for manipulation and biomechanical characterization of human red blood cells (RBCs). We first demonstrate the effectiveness of the robot-tweezers system in manipulation of micro-beads, which is followed by stretching RBCs to different levels of deformations. The whole manipulation process is conducted with visual guidance and position feedback control, where the cell stretching direction is determined automatically through image analysis. The relationship between the stretching force and the induced deformation is obtained through force calibration and image processing. To characterize the mechanical properties of RBCs from the obtained experimental results, a mechanical model based cell property characterization strategy is introduced. Comparing the modeling results to the experimental data, the mechanical properties of human RBCs are characterized. In conclusion, this study demonstrates that the robotic manipulation technology with optical tweezers can be used to manipulate biological cells, and further, to characterize the biomechanical properties based on the cell mechanical model.**

I. Introduction

MICROMANIPULATION of biological cells has attracted considerable attentions in recent years. This technology utilizes contact or noncontact interaction manner to manipulate cells and has been widely used in many biomedical fields such as cell transportation [1], cell sorting or isolation [2], cell injection [3], cell stretching [4], cell properties characterization [5], and so on.

Some experimental techniques have emerged as effective tools to manipulate cells and further measure their mechanical properties, which include micropipette aspiration [6], atomic force microscope [7], cell injection [8], cell poker [9], optical tweezers [4], and optical stretcher [10]. Most of the cell manipulations, however, are performed manually. Increasing demands for both high precision and high throughput in cell manipulation highlights the need for automated processing with robotics technology. Benefiting from great advance in visual servoing, micro-force sensing and control, motion control and image processing, robotic manipulation has become a promising tool in manipulating biological objects. Li et al. [11] employed a global vision system and autofocusing algorithm to develop an automatic micromanipulation system. Kratochvil et al. [12] proposed a real-time rigid-body visual tracking method for more precise automated manipulation. Huang et al. [13, 14] incorporated a vision-based position and force control algorithm into a biomanipulation system for automated batch microinjection. Arai et al. adopted the virtual reality technology to develop a three-dimensional biomanipulation system [15], and subsequently proposed a synchronized laser manipulation technique to control the trajectories of multiple objects by a single laser [16].

Optical tweezers are known for the ability to impose force and deformation on a micro-object on the order of piconewton (pN, 10^{-12} N) and nanometer (nm, 10^{-9} m) in a noncontact manipulation manner. In this paper, we propose to integrate robotics technologies in motion control, visual feedback and image processing into the optical tweezers system for robotic manipulation of biological cells. Human red blood cells (RBCs) are chosen as example cells for manipulation. RBCs are responsible for the transport of oxygen and carbon dioxide. Any alteration of the cell mechanics may cause human diseases. The recent researches have shown that alterations of mechanical properties of RBCs may be associated with the onset and progression of some diseases [17].

In this paper, we first introduce the robotic manipulation system with optical tweezers, and then demonstrate the effectiveness of this system in robotic manipulation of micro-beads and human RBCs stretching. With visual feedback and motion control, RBCs can be manipulated and stretched to different levels of deformations under various trapping forces. The relationship between the imposed stretching force and the induced deformation can be obtained by force calibration and image processing. To extract the cell properties from the experimental results, a mechanical model based cell property characterization strategy is proposed by extending our previous work [18, 19]. By fitting the modeling results to the experimental data, mechanical properties of RBCs can be characterized. This study successfully demonstrates that the robotic manipulation technology with optical tweezers, in combination with cell mechanical modeling, can be used to characterize the biomechanical properties of biological cells.

II. Robotic Manipulation System

Fig. 1 shows the optical tweezers system, which mainly consists of a single laser trap, a motorized stage, and an assembled chamber. A diode laser source with wavelength of

This work was supported by a grant from Research Grants Council of the Hong Kong Special Administrative Region, China [Reference No. CityU 120709], UGC Special Equipment Grant [SEG_CityU 01], and a grant from City University of Hong Kong [Reference No. 9360131].

Y. Tan and D. Sun are with the Department of Manufacturing Engineering and Engineering Management, City University of Hong Kong, Kowloon, Hong Kong (e-mail: {youhuatan2, medsun}@cityu.edu.hk, tel: 852-3442 5277, fax: 852-3442 0172).

W. Huang is with the Department of Precision Machinery and Precision Instrumentation, University of Science and Technology of China, Hefei, China (e-mail: whuang@ustc.edu.cn).

J. Cheng and S. Cheng are with the Department of Biology and Chemistry, City University of Hong Kong, Kowloon, Hong Kong (email: {jcheng, bhcheng}@cityu.edu.hk).

808 *nm* has a maximum power of 2.0 W. The laser beam is reflected by a dichroic mirror into a 40× objective and focused on the observation plane. To minimize the possible optical damage, the laser beam is focused on the polystyrene bead that is attached to the cell. The biological sample is placed on a two-dimensional motorized stage driven by two DC motors (PI M-111.1DG, Germany) with a positioning accuracy of 50 *nm*. The motion of the stage can be well controlled by the guidance of visual feedback and a piezoelectric motor control [20]. All of the mechanical components are supported upon an anti-vibration table.

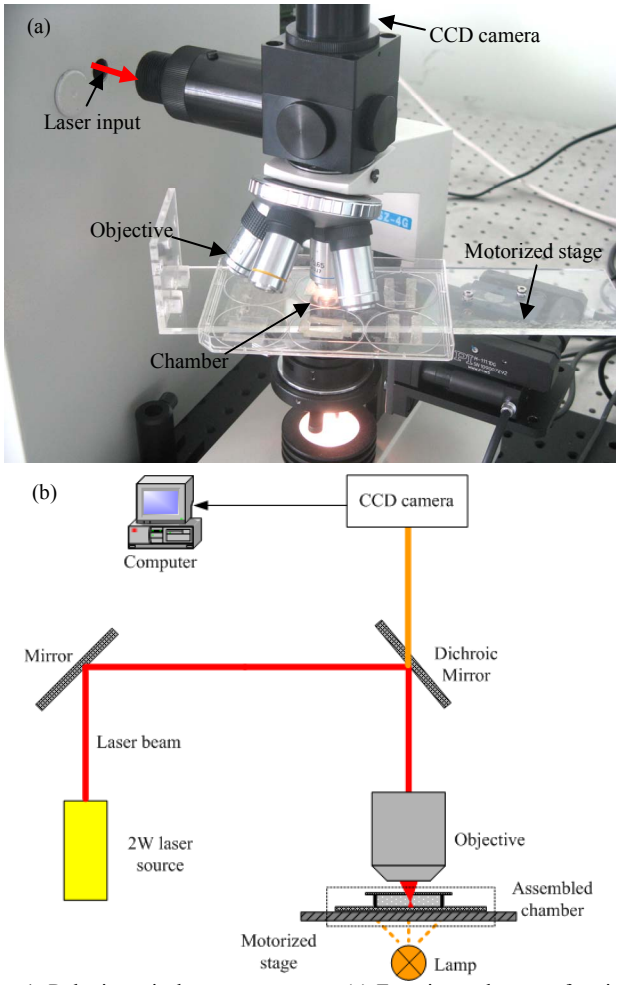

Fig. 1. Robotic optical tweezers system. (a) Experimental setup of optical tweezers system, (b) schematic diagram of optical tweezers system.

The mixture of RBCs and micro-beads was placed in a home-built chamber, which was assembled with usual microscopic slides and coverslips. All of the slides and coverslips were cleaned using ethanol. The coverslips were glued to the slide by superglue and sealed at the corners by nail polish. In the experiments of cell stretching, the surfaces of the chamber were bare glass. Once the adhesion between the cells and the beads was confirmed, the diluted mixture was injected into the chamber from an open end. Most of the RBCs were attached to the desired glass surfaces, and the unattached cells sank to the slide after inverting the chamber back. Then the chamber was ready for experiments. It should be noted that all the glass surfaces of the chamber were treated with 100 mg/ml bovine serum albumin (BSA, Sigma) to prevent the beads from sticking for micro-beads manipulation experiments.

III. Cell Property Characterization Strategy

In this section, a cell property characterization strategy is proposed. This strategy is based on the cell mechanical model, which is developed by extending our previous work [18, 19]. With the cell model, the deformation behavior of the cell during manipulation can be predicted. Also, the relationship between the manipulation force and the induced cell deformation can be obtained. Different cell properties correspond to different force-deformation curves. Comparing the modeling results to the experimental data, the mechanical properties of cells can be characterized.

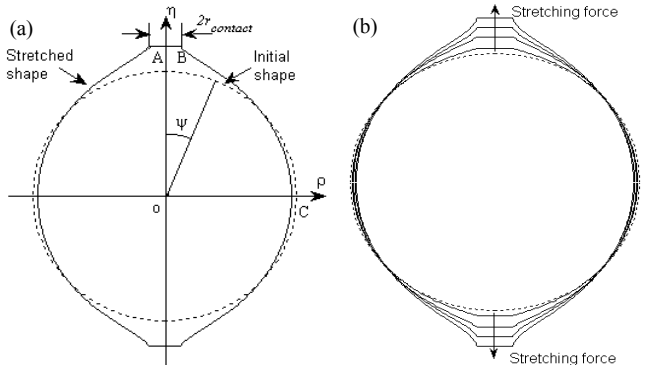

Fig. 2. (a) Coordinate definition before and after optical stretching, (b) the calculated deformed cell shapes after optical stretching.

The cell mechanical model is based on membrane theory, and utilizes the quasi-static equilibrium equations to describe the force balance in the meridian tangential and normal directions of the cell membrane, which are expressed by [18]

$$\frac{\partial T_1}{\partial \lambda_1}\lambda_1' + \frac{\partial T_1}{\partial \lambda_2}\lambda_2' = \frac{\rho'}{\rho}(T_2 - T_1) \quad (1)$$

$$K_1 T_1 + K_2 T_2 = P \quad (2)$$

where T_1 and T_2 are the principal tensions, λ_1 and λ_2 are the principal stretch ratios, K_1 and K_2 are the principal curvatures. The indices 1 and 2 refer to the corresponding component in the meridian and circumferential directions of the deformed membrane, respectively. P is the external pressure acting on the membrane in the normal direction. ρ is the transverse coordinate after deformation, as shown in Fig. 2 (a). The prime denotes the derivative with respect to the angle ψ.

Mooney-Rivlin material has been widely used to represent the deformation behavior of cell membranes [18, 21, 22]. Here we adopted it to model the characteristics of RBCs. The principal tensions T_1 and T_2 can be derived as follows

$$\begin{cases} T_1 = 2h_0 C(\dfrac{\lambda_1}{\lambda_2} - \dfrac{1}{(\lambda_1\lambda_2)^3})(1+\alpha\lambda_2^{\,2}) \\ T_2 = 2h_0 C(\dfrac{\lambda_2}{\lambda_1} - \dfrac{1}{(\lambda_1\lambda_2)^3})(1+\alpha\lambda_1^{\,2}) \end{cases} \quad (3)$$

where C and α are material constants, h_0 is the initial thickness of RBC biomembrane. For homogeneous, isotropic, and incompressible elastic material, $C = E/6(1+\alpha)$, where E denotes elastic modulus.

Since it is difficult to exactly define the interactions in the contact areas between the RBC and its exterior, we simplify this problem by assuming that the interactions in both the contact areas are similar. This approximation makes the deformed cell shape axisymmetric as reported by Suresh et al. [17]. Due to dual symmetry, only a quarter of the deformed cell shape is needed to be analyzed. The standard 4th order Runge-Kutta method is adopted to solve the equilibrium equations with the boundary conditions and volume conservation constraint. The solution procedure is similar to that in [18, 19, 21]. After numerical solution, the deformed cell shapes can be calculated as shown in Fig. 2 (b). The force and the cell deformation can be expressed as follows

$$F = T_{1C} \cdot 2\pi\rho_C - P\pi\rho_C^{\,2} \quad (4)$$

$$d = 2r_0 - 2\eta_B \quad (5)$$

where r_0 is the initial radius of RBCs. Given the material parameters in equation (3), the force-deformation relationship can be determined. With the calculation method reported in [5], the most appropriate material parameters can be obtained to minimize the deviation between the experiments and the modeling results. Subsequently, the cell properties can be characterized.

IV. Stretching of Human RBCs

In this section, the robotic manipulation system is utilized to stretch human RBCs.

A. Materials preparation and force calibration

Fresh blood was drawn from healthy donors by fingertip prick. RBCs were isolated from the blood sample via centrifugation. In parallel, streptavidin-coated polystyrene beads with radius of 1.55 μm (Bangs Lab., Fishers, IN) were rinsed and incubated with 1 mg/ml biotin conjugated concanavalin A (Con A, Sigma) at 4 $^\circ C$ for 40 minutes. The prepared beads were then added to the RBCs and incubated at 25 $^\circ C$ for one hour to allow the adhesion between the beads and RBCs. Once the adhesion was confirmed under an optical microscope, the mixture was diluted in 0.5 % hypotonic sodium chloride buffer to allow the RBCs to get swollen with spherical shapes.

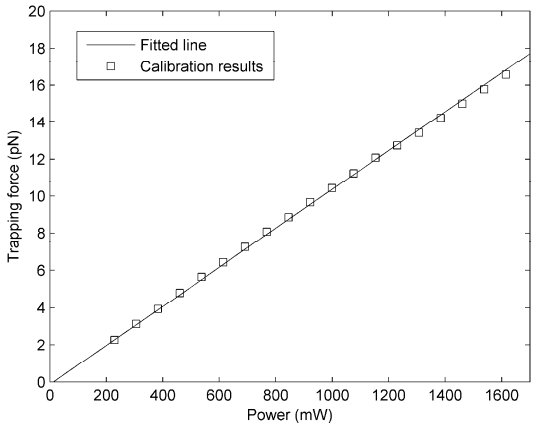

Fig. 3. Optical force calibration results by trapping a polystyrene bead with radius of 1.55 μm at the separation depth h = 5 μm from the coverslip.

During experiments, the trapping force cannot be measured directly. Thus it is necessary to perform a force calibration procedure. The usual viscous-drag-force calibration method is used here [4, 23]. When the flow velocity was increased up to a critical value beyond which the bead just escaped the laser trap, the bead achieved equilibrium, i.e., the trapping force equaled the viscous drag force. According to the Stokes law, the viscous drag force was expressed as [24]

$$F = \frac{6\pi R\eta_0 V_{crit}}{1 - 9/16(R/h) + 1/8(R/h)^3 - 45/256(R/h)^4 - 1/16(R/h)^5} \quad (6)$$

where R is the radius of the trapped bead, η_0 is the fluid viscosity ($\eta_0 = 1.01\times10^{-3}$ Pa.s at 25 $^\circ C$), V_{crit} is the critical velocity, h is the separation distance of the bead from the coverslip surface. Throughout the calibration and cell stretching experiments, h was kept to be 5 μm.

Fig. 3 shows the calibration results. At each laser power, 5 separated measurements were conducted and the obtained results were averaged. All the data can be fitted by a straight line, which coincides with the reported results [24].

B. Optical stretching of human RBCs by robotic manipulation

To stretch RBCs and minimize the potential optical damage, a micro-bead was adhered to the cell surface as a "handle". The laser beam was focused on the attached bead instead of the cell. Thus the micro-beads were manipulated directly by optical trap in the RBCs stretching experiments. Here, we first demonstrate the efficiency of micro-beads manipulation by optical tweezers. Fig. 4 shows the manipulation process. Through image processing, the contour and centroid of the trapped bead were obtained, which enabled real-time detection of the position of the bead. When the desired position was given, the moving direction of the motorized stage was determined along the line passing through the initial and the desired positions. Then the motions of the two-axis motorized stage were coordinated and controlled by a PID algorithm. With visual feedback, the trapped bead could move to the desired position, as shown in Figs. 4 (a)-(e). Note that when the moving velocity of the

motorized stage was lower than the critical value calculated from equation (6), the trap could hold the bead tightly as shown in Figs. 4 (a)-(e). As the velocity increased beyond this critical value, the bead escaped the trap as seen in Fig. 4 (f). It was easy to detect the escape of the bead when the center of the bead deviated from the center of the trap.

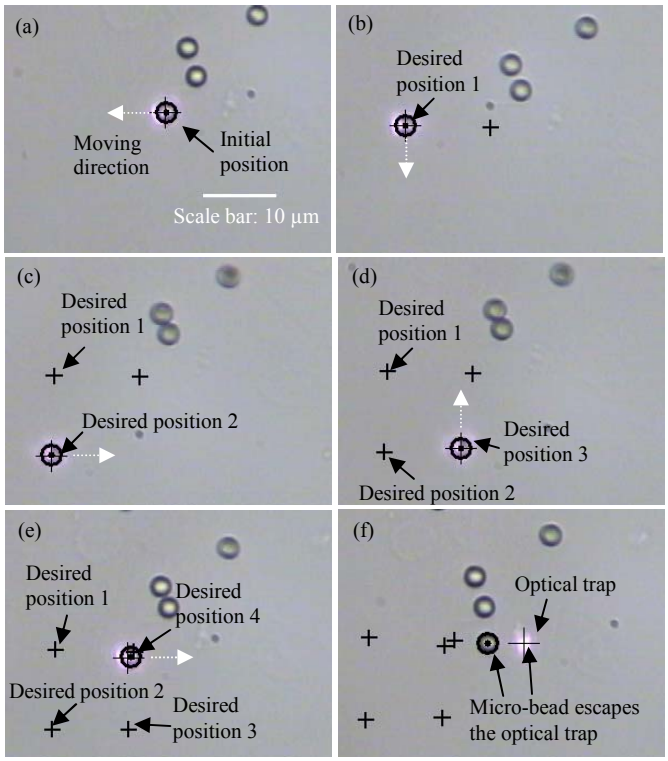

Fig. 4. Robotic manipulation process of micro-beads by optical tweezers. (a)-(e) the trapped bead moves automatically from the initial position to the desired position by optical tweezers, (f) the bead escapes the optical trap. The big and small crosses denote the center of the optical trap and the desired position of the bead. The black circle and dot indicate the contour and center of the trapped micro-bead, respectively. The moving directions are represented by the white arrows.

During cell stretching experiments, a small portion of a RBC was required to be anchored to the side wall of the chamber while the attached bead on the opposite side was captured by the optical trap as shown in Fig. 5, which could be achieved by reversing the chamber to let the RBCs settle down and adhere to the side wall of the chamber.

It is worth noting that the moving direction of the motorized stage is determined by image processing. Fig. 6 illustrates the determination process. Before cell stretching, a cell image was acquired and smoothed to suppress noises by convolved with a low-pass Gaussian filter. The Canny edge detector with adaptive thresholding [25] was employed to track the cell contour as shown in Fig. 6 (b). The centroids of the RBC and the attached bead were obtained via Hough transform [26], which were denoted by hollow and filled black dots in Fig. 6 (c), respectively. The moving direction was then determined to be along the line passing through these two centroids and moving away from the trap. Moreover, the contact areas between a cell and its exterior could also be measured through image processing. Fig. 6 (b) shows that the two contact areas were similar and varied slightly during the elongation, which verified the hypothesis assumed in the cell modeling. The contact radii were measured from the deformed cell which just achieved equilibrium and $r_{contact}$ was defined as the average of both of the contact radii.

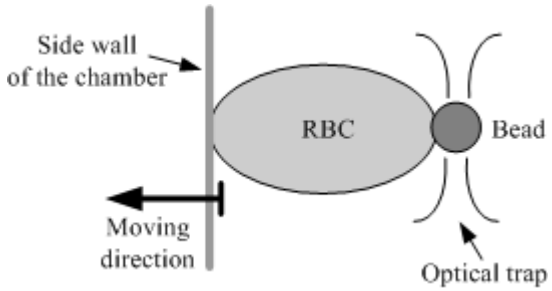

Fig. 5. A schematic graph of the stretching experiments where one side of the RBC is fixed onto the glass surface and the other side is held by the laser trap.

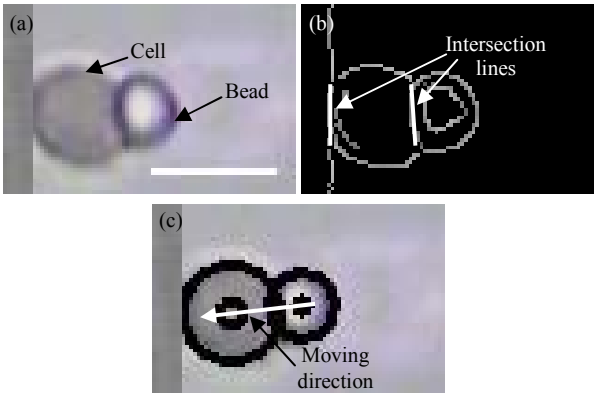

Fig. 6. Determination of the moving direction of the motorized stage through image processing before RBCs stretching experiments. (a) original image, (b) cell edge detection, (c) centroids detection and moving direction determination. The hollow and filled black dots denote the centroids of the cell and the bead, respectively. The moving direction is along the line which passes through these two centroids as marked by the white arrow. The white line represents the intersection line between the cell and the bead.

In summary, cell stretching procedures are generalized as follows. First, the position of the attached bead was determined by image analysis. The motion of the motorized stage was controlled and the bead was then trapped by the laser beam. After determination of the moving direction, the two axes of the stage were controlled, which enabled the stage to move in the specific direction. The maximum moving velocity of the stage was regulated to be less than 2 μm/s to minimize the extra viscous drag force exerted on the trapped bead by the flowing fluid. With visual feedback, the distance between the centers of the trapped bead and the optical trap could be acquired in real time. When the bead was observed to escape from the optical trap, the motion of the stage stopped. After adjusting the laser power, the operation can be resumed.

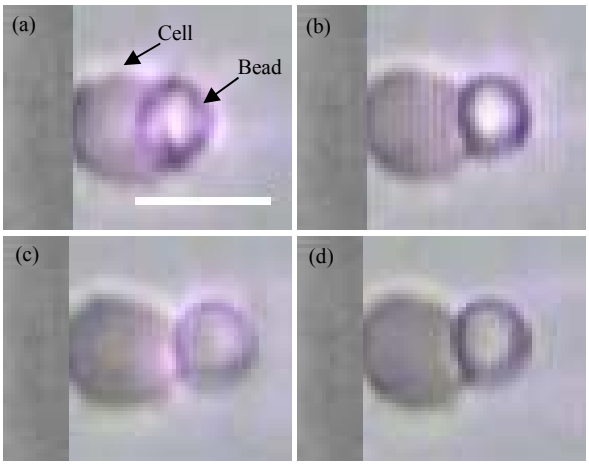

Fig. 7. Stretching process of a swollen RBC. (a) before stretching, (b) during stretching, (c) stretched to the maximum deformation, (d) the bead escapes the laser trap. Scale bar is 5 μm.

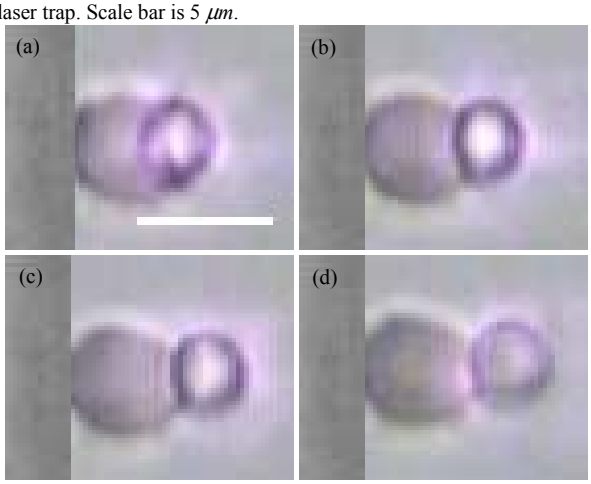

Fig. 8. The deformed cell shapes of a swollen RBC at different levels of stretching forces: (a) 0 pN, (b) 3 pN, (c) 8 pN, (d) 15 pN. Scale bar is 5 μm.

Fig. 7 shows the stretching process of RBCs at a given laser power. For each stretching experiment, the RBC was stretched to different levels of deformations over a range of laser powers as shown in Fig. 8. The stretched cell shapes were captured for estimation of the cell deformation when the trap just could not hold the bead as shown in Fig. 7 (c). The trapping force could be acquired from the calibrated force-power relationship at different levels of laser powers. Therefore, the relationships between the stretching force and the induced axial deformation were obtained at various laser powers.

V. Cell Property Characterization

The trapping forces and the cell deformations were obtained from force calibrations and image processing, respectively. Fig. 9 shows the experimental results for RBCs stretching under various stretching forces. To obtain each data, 10 separated stretching tests were conducted and the acquired results were averaged. In parallel, several parameters should be initialized in the proposed cell mechanical model. For example, the membrane thickness of human RBCs was taken to be 20 *nm* [27]. The typical value of $r_{contact}$ was measured to be between 0.75 μm and 0.9 μm. The cell radius of the swollen RBC was 3.3 μm. With these known quantities, the equilibrium equations (1) and (2) were solved by the Runge-Kutta method. The modeling relationship between the trapping force and the induced deformation could be calculated based on equations (4) and (5). To characterize the cell properties from the experimental data, the identification procedure reported in [5] was used. When the deviation parameter between the experiments and the cell modeling was minimized, the most appropriate values of C and α in equation (3) could be obtained. The elastic modulus E was then calculated by the relation $E = 6C(1+\alpha)$.

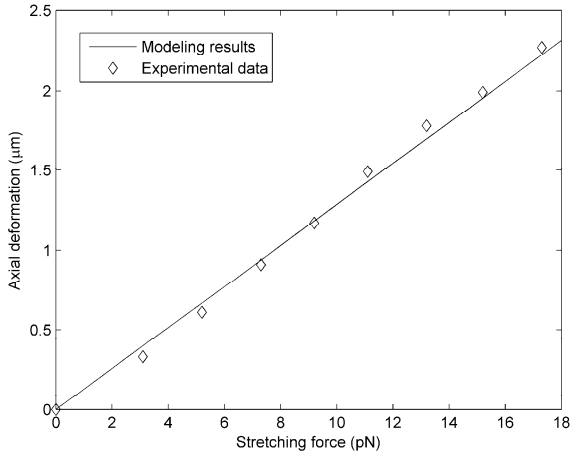

Fig. 9. Comparisons of the experimental data and the modeling results.

Through comparisons, it is found that the modeling results are in good agreement with the experimental data when the elastic modulus E is given as $1.58 \pm 0.4\ kPa$. As the shear modulus μ is usually reported in the literature rather than the elastic modulus, we convert it by the relation $\mu = Eh_0 / 2(1+\nu)$ (ν is the Poisson ratio). In our study, since the biomembrane is assumed to be incompressible, i.e., $\nu = 0.5$, the shear modulus can be calculated as $10.5 \pm 2.7\ \mu N/m$. The acquired mechanical properties of the swollen RBCs are consistent with the reported values, e.g., the shear modulus of RBCs in hypotonic condition is in the range of $2.5 \sim 10 \mu N/m$ [23, 28].

It is also found in Fig. 9 that the relationship between the stretching force and the cell deformation is quasi-linear. The reason may be that human RBCs are deformed in the region of relatively small forces. When the stretching force increases, the deformation behaviors of RBCs will become nonlinear and cell stiffening occurs [4, 23].

In conclusion, the robotic manipulation technology with optical tweezers is demonstrated to be effective in cell manipulation, and further, in mechanical properties characterization. Based on the proposed cell model, the shear modulus of swollen RBCs is characterized. This may have potential applications in the biomedical fields. Alterations of cell properties have been found in many diseases, such as cancer [29], malaria [17], sickle cell disease [30], and

diabetes mellitus [31]. The cell property characterization strategy developed in this paper can be used to measure the mechanical properties of cells obtained from patients with certain disease. After measurement at different stages of the disease, the variation trend of the cell property can be obtained. Therefore, taken the cell property as a biomarker, early detection of some incurable diseases, e.g., acute myeloid leukemia, may be possible. Thus this study has potential applications in the identification of diseased cells and may help medical diagnosis of some human diseases.

VI. CONCLUSIONS

In this paper, robotics technology is integrated into optical tweezers system for automatic manipulation of biological cells. We first introduce the robotic manipulation system with optical tweezers in our laboratory, and then demonstrate the effectiveness of this technology in manipulation of micro-beads. With visual feedback and motion control, human RBCs are manipulated and stretched to different levels of deformations. The relationship between the stretching force and the induced cell deformation is obtained through force calibration and image analysis. To extract the mechanical properties from the experimental data, a mechanical model based cell property characterization strategy is proposed. With this strategy, the mechanical properties of human RBCs can be characterized. In conclusion, this study demonstrates that optical tweezers based robotic manipulation technology in combination with cell modeling method can be used to characterize the mechanical properties of biological cells.

REFERENCES

[1] P. C. H. Li and D. J. Harrison, "Transport, manipulation, and reaction of biological cells on-chip using electrokenetic effects," Anal. Chem., vol. 69, pp. 1564-1568, 1997.

[2] F. Arai, A. Ichikawa, M. Ogawa, T. Fukuda, K. Horio, and K. Itoogawa, "High-speed separation system of randomly suspended single living cells by laser trap and dielectrophoresis," Electrophoresis, vol. 22, pp. 283-288, 2001.

[3] P. Kallio and J. Kuncova, "Manipulation of living biological cells: challenges in automation," presented at the Workshop on Microrobotics for Biomanipulation in IEEE/RSJ Int. Conf. on Intelligent Robots and Systems, 2003.

[4] M. Dao, C. T. Lim, and S. Suresh, "Mechanics of the human red blood cell deformed by optical tweezers," J. Mech. Phys. Solids, vol. 51, pp. 2259-2280, 2003.

[5] Y. Tan, D. Sun, and W. Huang, "Mechanical modeling characterization of biological cells using microrobotics cell injection test bed," Proc. IEEE/RSJ Int. Conf. on Intelligent Robots and Systems, pp. 4337-4342, October 2009.

[6] R. M. Hochmuth, "Micropipette aspiration of living cells," J. Biomech., vol. 33, pp. 15-22, 2000.

[7] S. Sen, S. Subramanian, and D. E. Discher, "Indentation and adhesive probing of a cell membrane with AFM: theoretical model and experiments," Biophys. J., vol. 89, pp. 3203-3213, 2005.

[8] Y. Xie, D. Sun, C. Liu, H. Y. Tse, and S. H. Cheng, "A force control approach to a robot-assisted cell microinjection system," Int. J. Robot. Res., vol. 29, 2010.

[9] B. Daily and E. L. Elson, "Cell poking: determination of the elastic area compressibility modulus of the erythrocyte membrane," Biophys. J., vol. 45, pp. 671-682, 1984.

[10] J. Guck, R. Ananthakrishnan, H. Mahmood, T. J. Moon, C. C. Cunningham, and J. Kas, "The optical stretcher: a novel laser tool to micromanipulate cells," Biophys. J., vol. 81, pp. 767–784, 2001.

[11] X. D. Li, G. Zong, and S. Bi, "Development of global vision system for biological automatic micromanipulation system," Proc. IEEE Int. Conf. on Robotics and Automation, vol. 1, pp. 127-132, 2001.

[12] B. E. Kratochivil, L. X. Dong, B. J. Nelson, "Real-time rigid-body visual tracking in a scanning electron microscope," Int. J. Robot. Res., vol. 28, pp. 498-511, 2009.

[13] H. B. Huang, D. Sun, J. K. Mills, and S. H. Cheng, "Robotic cell injection system with vision and force control: Towards automatic batch biomanipulation," IEEE Trans. Robot., vol. 25, no. 3, pp. 727-737, June 2009.

[14] H. B. Huang, D. Sun, J. K. Mills, and W. J. Li, "Visual-based impedance control of out-of-plane cell injection systems," IEEE Trans. Autom. Sci. Eng., vol. 6, no. 3, pp. 565-571, July 2009.

[15] F. Arai, A. Kawaji, P. Luangjarmekorn, T. Fukuda, and K. Itoigawa, "Three-dimensional bio-manipulation under the microscope," Proc. IEEE Int. Conf. on Robotics and Automation, pp. 604-609, 2001.

[16] F. Arai, K. Yoshikawa, T. Sakami, and T. Fukuda, "Synchronized laser micromanipulation of multiple targets along each trajectory by single laser," Appl. Phys. Letts., vol. 85, pp. 4301-4303, 2004.

[17] S. Suresh, J. Spatz, J. P. Mills, A. Micoulet, M. Dao, C. T. Lim, M. Beil, and T. Seufferlein, "Connections between single-cell biomechanics and human disease states: gastrointestinal cancer and malaria," Acta Biomaterialia, vol. 1, pp. 15-30, 2005.

[18] Y. Tan, D. Sun, W. Huang, and S. H. Cheng, "Mechanical modeling of biological cells in microinjection," IEEE Trans. NanoBioSci., vol. 7, no. 4, pp. 257-266, Dec. 2008.

[19] Y. Tan, D. Sun, and W. Huang, "Mechanical modeling of red blood cells during optical stretching," J. Biomech. Eng.-Trans ASME, vol. 132, no. 4, pp. 044504, April 2010.

[20] D. Sun, J. B. Liu, and X. Ai, "Modeling and performance evaluation of traveling-wave piezoelectric ultrasonic motors with analytical method," Sens. Actuator A-Phys., vol. 100, pp. 84-93, 2002.

[21] Y. Tan, D. Sun, J. Wang, and W. Huang, "Mechanical characterization of human red blood cells under different osmotic conditions by robotic manipulation with optical tweezers," IEEE Trans. Biomed. Eng., vol. 57, no. 7, pp. 1816-1825, 2010.

[22] Y. Tan, D. Sun, W. Huang, and S. H. Cheng, "Characterizing mechanical properties of biological cells by microinjection," IEEE Trans. NanoBioSci., vol. 9, no.3, 2010.

[23] S. Henon, G. Lenormand, A. Richert, and F. Gallet, "A new determination of the shear modulus of the human erythrocyte membrane using optical tweezers," Biophys. J., vol. 76, pp. 1145-1151, 1999.

[24] K. Svoboda and S. M. Block, "Biological applications of optical forces," Annu. Rev. Biophys. Biomol. Struct., vol. 23, pp. 247-285, 1994.

[25] W. Zhi, Q. Li, S. Zhong, and S. He, "Fast adaptive threshold for the canny edge detector," Proc. SPIE, vol. 6044, pp. 60441Q1-6, 2005.

[26] R. C. Gonzalez and P. Wintz, "Digital image processing," Addison-Wesley, 1987

[27] T. Fischer, "Role of spectrin in cross bonding of the red cell membrane," Blood Cell, vol. 13, pp. 377-394, 1988.

[28] R. M. Hochmuth and R. E. Waugh, "Erythrocyte membrane elasticity and viscosity," Annu. Rev. Physiol., vol. 49, pp. 209-219, 1987.

[29] S. E. Cross, Y. S. Jin, J. Y. Rao, and J. K. Gimzewski, "Nanomechanical analysis of cells from cancer patients," Nat. Nanotechnol., vol. 2, pp. 780-783, 2007.

[30] G. B. Nash, C. S. Johnson, and H. J. Meiselman, "Mechanical properties of oxygenated red blood cells in sickle cell (HbSS) disease," Blood, vol. 63, pp. 73-82, 1984..

[31] K. Tsukada, E. Sekizuka, C. Oshio, and H. Minamitani, "Direct measurement of erythrocyte deformability in diabetes mellitus with a transparent microchannel capillary model and high-speed video camera system," Microvasc. Res., vol. 61, pp. 231-239, 2001.